Autoregressive model-based reconstruction of quantitative acoustic maps from RF signals sampled at innovation rate

J-H. Kim[1], J. Mamou[2], D. Kouamé[1], A. Achim[3], and A. Basarab[1]

[1]*IRIT UMR CNRS 5505, University of Toulouse, CNRS, INPT, UPS, UT1C, UT2J, France*
[2]*Frederic L. Lizzi Center for Biomedical Engineering, Riverside Research, New York, NY 10038, USA*
[3]*Visual Information Lab, SCEEM, University of Bristol, UK*

***Abstract*—The principle of quantitative acoustic microscopy (QAM) is to form two-dimensional (2D) acoustic parameter maps from a collection of radiofrequency (RF) signals acquired by raster scanning a biological sample. Despite their relatively simple structure consisting of two main reflections, RF signals are currently sampled at very high frequencies, *e.g.*, at 2.5 GHz for QAM system employing a single-element transducer with a center frequency of 250-MHz. The use of such high sampling frequencies is challenging because of the potentially large amount of acquired data and the cost of the necessary analog to digital converters. Based on a parametric model characterizing QAM RF signals, the objective of this paper is to use the finite rate of innovation (FRI) framework in order to significantly reduce the number of acquired samples. This is directly fed into a state-of-the-art autoregressive (AR)-based method to estimate the model parameters, which finally leads to the reconstruction of accurate 2D maps. The combination of FRI and AR model for sampling and parametric map recovery allows decreasing the required number of samples per RF signal up to a factor of 18 compared to a conventional approach, with a minimal accuracy loss of quantitative acoustic maps, as proven by visual evaluations and numerical results, *i.e.* PSNR of 24.50 dB and 24.51 dB for the reconstructed speed of sound map and acoustic impedance map.**

***Index Terms*—Scanning Acoustic Microscopy, finite rate of innovation, auto-regressive model.**

I. Introduction

Quantitative Acoustic Microscopy (QAM) uses high frequency ultrasound waves to investigate the mechanical properties of biological tissues at a microscopic scale [1]–[4]. Currently, the acquisition process in QAM requires a raster scan of the sample, resulting into a large amount of RF data acquired by transmitting short ultrasound pulses into a thin section of soft tissue affixed to a microscopy slide. At each spatial position, the received RF echo consists of two main reflections due to the water-tissue and tissue-glass interfaces. These reflections are time-shifted, frequency-attenuated, and amplitude-decayed versions of a reference reflection signal obtained from a water-glass interface. Two-dimensional (2D) acoustic maps are thus estimated from an RF data cube using a state-of-the-art inverse model based on an autoregressive (AR) model for each RF signal [5]. Despite their limited degrees of freedom, QAM RF signals are currently sampled beyond the Nyquist rate. For example, within our 250-MHz imaging system with 6-dB bandwidth of 300 MHz, RF signals are sampled at 2.5 GHz. This arouses a number of practical issues, such as a large amount of acquired data or the cost and the complexity of the A/D converters and other fast electronic components. In our previous study [6], we proved that, in the spatial domain, applying the compressed sensing framework with an approximate message passing reconstruction algorithm to the QAM data acquisition enables a significant decrease in the amount of RF signals acquired and the scanning time. This work proposes a sampling scheme in the temporal domain able to drastically reduce the number of samples per RF signal required to reconstruct accurate acoustic maps in QAM [7]. The proposed approach is based on the finite rate of innovation (FRI) theory [8] that provides theoretical guarantees for reconstructing non-bandlimited parametric signals, such as train of Diracs, from a small number of samples taken at the innovation rate. The class of signals subjected to the FRI framework, so called FRI signals, can be commonly modeled as a signal in union of subspaces spanned by a limited set of parameters with a known basis, instead of a single linear vector space forcing an input signal to be bandlimited [9]. As such, given the basis function as a prior information, the novel sampling process carries out a uniform sampling at a remarkably reduced sampling rate, *i.e.* the rate of innovation, corresponding to the degree of freedom able to perfectly characterize the considered signal. The reconstruction strategy is equivalent to identifying the innovation part of the signal, typically using the annihilating filter technique [10], the matrix pencil method [11] or total least-squares [12]. In this regard, taking into account the aforementioned nature of QAM RF signals, namely parametrically expressed by two pulses varied with amplitude decay, time delay and frequency dependent attenuation of a known pulse, the low rate sampling scheme based on the FRI manner could contribute to a significant reduction of the number of samples. Nevertheless, it should be noted that this signal has an additional degree of freedom, *i.e.*, the frequency attenuation in comparison with signal models normally considered in FRI context, which is likely to be an intractable parameter for existing estimators generally employed in FRI studies. Thus, in order to successfully introducing FRI sampling framework to our signal model, we propose a novel technique, *i.e.*, FRI

sampling scheme combined with AR model-based estimation. The proposed sampling and reconstruction methods for QAM RF signals are evaluated on experimental data obtained from a chicken tendon. The resulting acoustic parameter maps are compared to those computed directly from the fully sampled RF data cube. The simulation results demonstrate that the sampling frequency currently used within existing scanners can be reduced by a factor of 18 (*i.e.*, 15.6% of Nyquist rate) without degrading the quality of the 2D acoustic maps.

The remainder of this paper is structured as follows. Section II briefly presents the necessary theoretical background of QAM technology and in particular the parametric model used for RF signals, and the basic theory behind sampling and reconstruction of FRI signals. Section III introduces the proposed QAM RF signal sampling scheme and reconstruction method. Results are reported in Section IV, before conclusive remarks and perspectives in Section V.

II. Theoretical background

A. Signal model in quantitative acoustic microscopy

In QAM, a high-frequency (> 50 MHz), single-element, spherically-focused (*e.g.*, F-number < 1.3) transducer transmits a short ultrasound pulse and receives the RF echo signal reflected from the sample which consists of a thin section of soft tissue affixed to a microscopy slide. The echo RF signal denoted by $S(t)$ in (1) is composed of two main reflections, $S_1(t)$ and $S_2(t)$, as illustrated in Fig. 1. $S_1(t)$ originates from the interface between the coupling medium (degassed saline) and the specimen, and $S_2(t)$ from the interface between the specimen and the glass substrate.

$$S(t) = S_1(t) + S_2(t) \tag{1}$$

Estimating acoustic parameters from $S(t)$ basically requires the knowledge of a reference signal, denoted by $S_0(t)$ in Fig. 1(a), obtained in practice from a region devoid of sample. Echoes $S_1(t)$ and $S_2(t)$ can be further linked to the reference signal $S_0(t)$ through amplitude decays $a_{1,2}$ and time delays $t_{1,2}$. Moreover, due to a round trip flight inside the sample, $S_2(t)$ experiences an additional effect of frequency dependent attenuation represented by $(*)$. This observation on the physical phenomena allows one to build a more explicit formula of the received RF signals, which paves the way for introducing the FRI sampling and reconstruction in QAM imaging:

$$S(t) = a_1 S_0(t - t_1) + a_2 S_0^{(*)}(t - t_2), \tag{2}$$

At each scan location, the RF data is digitized, saved, and processed offline to yield values of speed of sound ($\boldsymbol{c}$), acoustic impedance ($\boldsymbol{Z}$) and attenuation coefficient ($\boldsymbol{\alpha}$) [4]. For doing these, the ratio between the Fourier transforms of the sample signal (S) and the reference signal (S_0) is computed, and fit to a forward model to estimate the time lags of S_1 and S_2 with respect to S_0. These time differences are exploited to determine $\boldsymbol{c}$ and the tissue thickness ($\boldsymbol{d}$ in Fig. 1(a)) corresponding to the scanned location of the sample. The forward model fit also provides the amplitude of S_1, which is used to estimate $\boldsymbol{Z}$ in the sample. Finally, $\boldsymbol{\alpha}$ is obtained from the previously-estimated time delay of S_2 and the tissue thickness $\boldsymbol{d}$ [4]. More details about the computation of these acoustic parameter maps are given in Section IV.

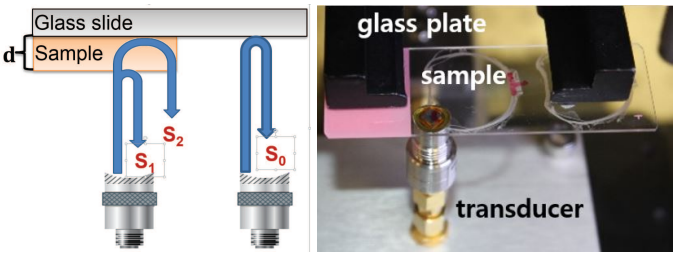

(a) (b)

Fig. 1. Illustrative working principle of QAM (a) and transducer (b)

B. FRI signal sampling and reconstruction

Signals with a limited number of degrees of freedom occur in various applications such as astronomy, radar or medical imaging [13]–[17]. Generally called signals with FRI, they are typically expressed as a τ-periodic parametric form as follow:

$$x(t) = \sum_{m \in Z} \sum_{l=1}^{L} a_l h(t - t_l - m\tau), \tag{3}$$

where $h(t)$ is a possibly non-bandlimited pulse supposed to be known and repeated L times at the time instants t_l and scaled by the amplitudes a_l. Starting from the seminal paper of Vetterli *et al.* [8], a rich literature exists on the reconstruction of these kinds of signals from a limited number of samples. In contrast to the classical sampling theory based on the celebrated Shannon-Nyquist theorem that relates the number of samples required to the signal bandwidth, the number of measurements in FRI framework is dictated by the rate of innovation (ρ), *i.e.*, the number of parameters able to completely describe $x(t)$ over one period. Given the parametric representation in (3) of a signal of interest, the canonical FRI processes involve the design of a relevant sampling kernel and the development of effective recovery strategies, which will be addressed hereafter.

Construction of a proper sampling kernel: Finding appropriate sampling kernels has been vigorously carried out in several existing studies, *e.g.*, [8], [18]. As requirements commonly highlighted in these works, the sampling kernels adopted must be resilient to noise and have a compact support in time, and therefore should be able to ensure a stable and accurate reconstruction. Taking into account these aspects, exponential reproducing kernels $\varphi(t)$ are most frequently addressed in FRI literature [19], [20]:

$$\sum_{n \in \mathbb{Z}} c_{m,n} \varphi(t - n) = e^{\alpha_m t}, \tag{4}$$

where $c_{m,n}$ are proper coefficients able to reproduce complex exponentials, *i.e.* $e^{\alpha_m t}$ $(m = 0, \ldots, P)$ with complex value parameters α_m, via a linear combination of shifted versions of any function $\varphi(t)$. Importantly, when $\Phi(\alpha_m)$ represents the Laplace transform of $\varphi(t)$ evaluated at α_m, such kernels

necessarily satisfy $\Phi(\alpha_m) \neq 0$ and $\Phi(\alpha_m + 2j\pi l) = 0$ for $l \in Z\backslash\{0\}$ [21], and the coefficients $c_{m,n}$ are given by:

$$\begin{aligned} c_{m,n} &= \int_{-\infty}^{\infty} e^{\alpha_m t}\tilde{\varphi}(t-n)dt \\ &= \int_{-\infty}^{\infty} e^{\alpha_m x}e^{\alpha_m n}\tilde{\varphi}(x)dx = c_{m,0}e^{\alpha_m n}, \end{aligned} \tag{5}$$

where the dual analysis function $\tilde{\varphi}(t)$ is biorthogonal to $\varphi(t)$, *i.e.*, $\langle\tilde{\varphi}(t-n), \varphi(t-m)\rangle = \delta_{m-n}$ [22]. In order to guarantee a stable and accurate recovery, the FRI setting established in [20] imposes some conditions on the matrix consisting of the elements $c_{m,n}$, which is square and unitary and its condition number is one. Overall, the requirements are supported by $|c_{m,0}| = 1$ and α_m being purely imaginary exponents to be located on the unit circle.

Uniform sampling*:* Let x_n be a finite set of N samples acquired by low pass filtering and uniformly sampling $x(t)$ at intervals of T with a sampling kernel $\varphi(t)$.

$$x_n = \left\langle \underbrace{\sum_{l=1}^{L} a_l h(t-t_l)}_{\text{one period of } x(t)}, \varphi\left(\frac{t}{T} - n\right)\right\rangle \tag{6}$$

Estimating the unknown parameters from samples x_n*:* In order for relating the spectral estimation method to the estimation of the unknown parameters in (3), the uniformly sampled measurements x_n are transformed into a sequence of moments M_m taking advantage of (5) and (6) [20]:

$$M_m = \sum_{l=1}^{L} a_l u_l^m, \tag{7}$$

where $m = 0, \ldots, P$ and the sampling kernel's order corresponds to $P + 1 \geq 2L$. Determining both u_l's containing the time delays t_l and amplitudes a_l is subject to solving a classical problem in spectral analysis [10].

III. Material and Methods

A. Signal model

In QAM, RF signals consist of two main reflections plotted as the continuous line in Fig. 2 (a), which can be parametrically modeled with a reference RF pulse displayed with the dotted line in Fig. 2 (a). The non-attenuated reference pulse, denoted by $h(t)$ hereafter and corresponding to $S_0(t)$ in (2), is commonly measured, at the same time when the sample is scanned, from a region without sample, *i.e.* presenting only one water-glass interface [5]. It is thus assumed to be known. The two frequency attenuated versions of h are denoted by $h^{(1)}$ and $h^{(2)}$. Written in a τ-periodic version, the QAM RF signal model is as follows:

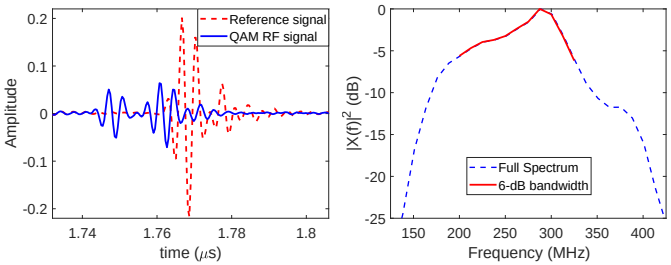

(a) (b)

Fig. 2. (a) Example of reference and QAM RF signals in the time domain, (b) Fourier transform of the reference signal in (a) highlighting the 6dB bandwidth.

$$\begin{aligned} x(t) &= \sum_{m\in Z}\sum_{l=1}^{2} a_l h^{(l)}(t - \Delta t_l - m\tau) \\ &\overset{(a)}{=} \sum_{k\in Z}\left\{\frac{1}{\tau}H\left[\frac{2\pi k}{\tau}\right]\sum_{l=1}^{2} a_l e^{\frac{-j2\pi k\Delta t_l - 2\pi k\beta_l}{\tau}}\right\} e^{\frac{j2\pi kt}{\tau}} \\ &\triangleq \sum_{k\in Z} X[k]\, e^{\frac{j2\pi kt}{\tau}}, \end{aligned} \tag{8}$$

where (a) is obtained applying the Poisson's summation formula [23], β_l, a_l and Δt_l stand respectively for the frequency attenuation coefficients, the amplitudes and the time delays. Without loss of generality, we assume β_1 equal to 0. Thus, the unknown parameters are a_1, a_2, Δt_1, Δt_2 and β_2. In (8), the last line represents the Fourier series expansion of $x(t)$, with $X[k]$ the Fourier series coefficients. By identification, one can easily connect $X[k]$ to the unknown parameters as follows:

$$X[k] = \frac{1}{\tau}H\left[\frac{2\pi k}{\tau}\right]\sum_{l=1}^{2} a_l e^{\frac{-j2\pi k\Delta t_l - 2\pi k\beta_l}{\tau}} \tag{9}$$

Assuming that one has access to a set of Fourier series expansion of $X[k]$, retrieving the unknown parameters from the sum of power series is closely related to the standard problem of identifying frequencies and amplitudes in spectral analysis [10]. The following sections explain how $X[k]$ can be obtained in practice, and the reconstruction method proposed is able to determine the model parameters defining QAM RF signals.

B. Sampling procedure

The sampling procedure used in this work was inspired by [17], where the stream of ultrasound pulses sampled at innovation rate was able to be exactly recovered using FRI framework. The main idea is to uniformly sample the demodulated QAM RF signal using a compactly supported Sum of Sincs (SoS) sampling kernel, and subsequently to relate these samples through a linear model to the Fourier series coefficients $X[k]$. In the Fourier domain, the SoS sampling kernel (denoted by $\varphi(t)$ in the time domain) is given by

$$\Phi(\omega) = \frac{\tau}{\sqrt{2\pi}}\sum_{k\in Z} b_k sinc\left(\frac{\omega}{\frac{2\pi}{\tau}} - k\right), \tag{10}$$

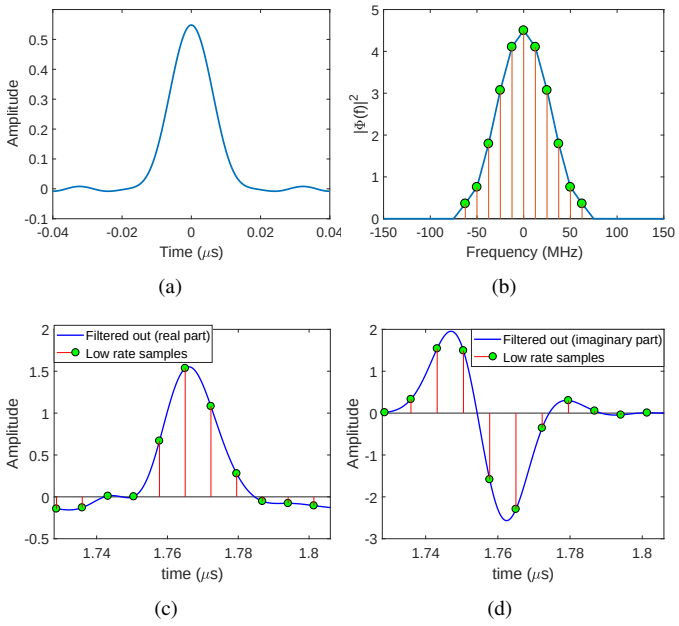

Fig. 3. Example of SoS sampling kernel is illustrated in temporal (a) and frequency domain (b). On the other hand, (c) and (d) show respectively real and imaginary parts after filtering and uniform sampling the demodulated RF signal using the SoS sampling kernel, where the applied innovation rate is 125MHz (equivalent to 11 samples over one period).

where b_k is a smoothing window (Hamming window was used in our experiments) and has a symmetric sequence of odd length, which leads to a real valued analog filter applicable to a continuous time domain. An example of SoS sampling kernel is shown in Fig. 3 (a-b), in both temporal and frequency domains, where the applied innovation rate is 125 MHz corresponding to 11 samples over one period. Note that the sampling kernel $\varphi(t)$ used within our sampling scheme is intrinsically a low pass filter, but the 6-dB bandwidth highlighted in Fig. 2 (b) to be sampled has the center frequency of 250 MHz. Therefore it should be shifted on the baseband prior to the low rate sampling. This requirement is accomplished by a standard I-Q demodulation [24], the outcome of which is filtered and sampled with the sampling kernel $\varphi(t)$ and a sampling period T respectively. We denote by $x[n]$ the sampled version of $x(t)$, and the process is detailed as follows.

$$\begin{aligned} x[n] = \langle x(t), \varphi(t-nT)\rangle &= \int_{-\infty}^{\infty} x(t)\varphi^*(t-nT)dt \\ &\overset{(a)}{=} \sum_{k\in Z} X[k] \int_{-\infty}^{\infty} e^{\frac{j2\pi kt}{\tau}} \varphi^*(t-nT)dt \\ &\overset{(b)}{=} \sum_{k\in Z} X[k] e^{\frac{j2\pi knT}{\tau}} \int_{-\infty}^{\infty} e^{\frac{j2\pi kt}{\tau}} \varphi^*(t)dt \\ &\overset{(c)}{=} \sum_{k\in Z} X[k] e^{\frac{j2\pi knT}{\tau}} \Phi^*\Big[\frac{2\pi k}{\tau}\Big], \end{aligned} \tag{11}$$

where (a) is obtained by substituting the result of the derivation in (8), (b) results from a change of variable, and $\Phi^*[2\pi k/\tau]$ in (c) denotes the discrete Fourier transform of $\varphi^*(t)$ evaluated at $[2\pi k/\tau]$. The superscript " $*$ " stands for complex conjugate. Fig. 3 (c-d) display, in the real and imaginary parts, samples filtered and uniformly decimated at an innovation rate after I-Q demodulating an RF signal. One may observe from (10) that $\Phi^*[2\pi k/\tau]$ is different from zero only for k's belonging to a finite set $\mathcal{K}$. Then, the summation, in the last line of (11), becomes finite ($k \in \mathcal{K}$ instead of $k \in \mathcal{Z}$), and can be rewritten as in (12). This nice property can be supported by any kernel satisfying the Strang-Fix condition [25], [26].

$$x[n] = \sum_{k\in\mathcal{K}} X[k] e^{\frac{j2\pi knT}{\tau}} \Phi^*\Big[\frac{2\pi k}{\tau}\Big]. \tag{12}$$

As a result, the Fourier series coefficients $X[k]$ can be computed from the digital samples $x[n]$ by applying the inverse of a correction matrix to the discrete Fourier transform of $x[n]$ as shown hereafter. (12) can be rewritten in a matrix-vector form as follows.

$$\mathbf{x} = \mathbf{VGX}, \tag{13}$$

where $\mathbf{x}$ and $\mathbf{X}$ are column vectors that gather respectively the discrete samples $x[n]$ and the Fourier coefficients $X[k]$ to be identified. Moreover, $\mathbf{V}$ and $\mathbf{G}$ are a Vandermonde matrix having $e^{(\frac{j2\pi knT}{\tau})}$ as (nk)th elements (discrete inverse Fourier transform matrix) and a diagonal matrix with $\Phi^*(\frac{2\pi k}{\tau})$ as main diagonal entries respectively. Based on (13), $\mathbf{X}$ is obtained by

$$\mathbf{X} = \mathbf{G}^{-1} DFT(\mathbf{x}), \tag{14}$$

where DFT stands for discrete Fourier transform. In the remainder of the paper, $X[k]$ plays a pivotal role to estimate the unknown parameters in (9). Note that the invertibility of matrix $\mathbf{G}$ is ensured by the choice of the sampling kernel and of the finite set $\mathcal{K}$ where $\Phi^*[2\pi k/\tau]$ is different from zero.

C. Reconstruction method

In QAM, the acoustic parameters of the scanned tissue are calculated based on the estimation of the amplitudes, time delays and frequency attenuation coefficients of each RF signal at each spatial location, following the signal model in (8) and more precisely its Fourier domain counterpart in (9). Within the proposed framework, these Fourier coefficients are directly estimated from the few samples acquired using SoS sampling kernel, as explained in the previous sections. The Fourier coefficients can be rewritten in a normalized form denoted by N_k containing only the terms associated with the parameters to be estimated, obtained by dividing $X[k]$ by $\frac{1}{\tau}H[2\pi k/\tau]$ in

$$\begin{aligned} N_k &= \sum_{l=1}^{n} a_l \{\exp[2\pi\Delta f(-\beta_l - j\Delta t_l)/\tau]\}^k \\ &= \sum_{l=1}^{n} a_l \lambda_l^k, \end{aligned} \tag{15}$$

where Δf and n are the step size leading to discrete frequencies, *i.e.* $f_k = k\Delta f$ and the number of pulses to be reconstructed respectively, and λ_l stands for $\exp[2\pi\Delta f(-\beta_l - j\Delta t_l)/\tau]$. Thus, the parameters of the model in (8) can be directly estimated by solving this problem without the need of reconstructing the RF signal. The estimation is accomplished

making use of an AR model, which unlike the previous setup in (9) supposes that QAM RF signals are composed of more than two reflections ($n \geq 2$) in order for providing robustness and stability to noise and estimation artifacts. Introducing the error term and the AR coefficients denoted by respectively ϵ and s, the AR inverse model for QAM proposed is formulated as follow:

$$N_k = \sum_{i=1}^{n} s_i N_{k-i} + \epsilon_k, \tag{16}$$

For the practical implementation, (16) is rewritten in matrix-vector form as:

$$\mathbf{n} = -\mathbf{R}\mathbf{s} + \boldsymbol{\epsilon}, \tag{17}$$

where provided that the normalized coefficients N_k are computed at the frequencies ranging from $k_{\text{max}}\Delta f$ to $k_{\text{min}}\Delta f$, $\mathbf{n}$ is the column vector of length $(k_{\text{max}} - k_{\text{min}} + 1 - n)$ representing the values of N_k from $(k_{\text{min}} + n)$ to k_{max}, $\mathbf{R}$ is the matrix of size $(k_{\text{max}} - k_{\text{min}} + 1 - n)$ by n whose entries are determined by N_{k-i}, and $\boldsymbol{\epsilon}$ is the column vector of length $(k_{\text{max}} - k_{\text{min}} + 1 - n)$ composed of the values ϵ_k from $(k_{\text{min}}+n)$ to k_{max}. Together with the process to find the solution to the AR coefficients $\mathbf{s}$, the great details regarding further derivations are presented in [5], and therefore in what follows we briefly summarize the remaining steps. The AR model coefficients s_i are estimated by a least-square approach (Eq. (14) in [5]). Then, the coefficients λ_l are determined by the roots of polynomials formed from the AR model coefficients (Eq. (18) in [5]). Subsequently, the coefficients a_l are obtained using a least-square approach (Eq. (20) in [5]). Among the n pairs of λ_l and a_l estimated, we select the two sets of parameters corresponding to the echoes reflected from the water-tissue and tissue-glass interfaces (see Section II.C.3 in [5]).

D. *Computation of acoustic parameters*

From the signal model parameters estimated as described in the previous section, speed of sound ($\boldsymbol{c}$), acoustic impedance ($\boldsymbol{Z}$) and attenuation ($\boldsymbol{\alpha}$) are computed as follows, where without loss of generality we assumed the water-tissue and tissue-glass signals are represented by (λ_1, a_1) and (λ_2, a_2), respectively.

$$c = c_w \frac{\text{imag}(\log(\lambda_1))}{\text{imag}(\log(\lambda_1)) + \text{imag}(\log(\lambda_2))}, \tag{18}$$

where $\boldsymbol{c}_w$ is the known speed of sound in the water used as a coupling fluid between the transducer and the sample.

$$\alpha = \frac{\text{real}(\log(\lambda_2))}{2d\Delta f}, \tag{19}$$

where $\boldsymbol{d}$ is the tissue thickness estimated by

$$d = \frac{c_w}{2} \frac{\text{imag}(\log(\lambda_1))}{\Delta f}, \tag{20}$$

$$Z = Z_w \frac{1 + \frac{a_1}{R_{wg}}}{1 - \frac{a_1}{R_{wg}}}, \tag{21}$$

where R_{wg} is the known pressure reflection coefficient between water and glass and defined in Eq. (34) in [5].

E. *Experimental data and QAM system*

To evaluate the FRI-based AR approach, experimental QAM data were acquired from a chicken tendon sample using a QAM system equipped with a 250 MHz center frequency transducer. A fresh chicken tendon was fixed in formalin while loaded longitudinally then cryosectioned (16-μm thick) and affixed to a microscopy slide [27]. The RF data cube was obtained by raster scanning the microscopy slide in two dimensions using 2-μm steps between adjacent scan lines. At each scan location, the RF signal was sampled at 2.5 GHz. The resulting RF data cube was of size $501 \times 501 \times 200$ RF samples. The QAM system has been described in great details in previous publications (see, *e.g.*, [2], [3], [28]) which were committed to identification of various elastic properties of soft tissues, *i.e.* attenuation ($\boldsymbol{\alpha}$), speed of sound ($\boldsymbol{c}$), acoustic impedance ($\boldsymbol{Z}$), bulk modules ($\boldsymbol{B}$) and mass density ($\boldsymbol{\rho}$). The -20 dB bandwidth of the QAM system extended to approximately 400 MHz. Therefore, in what follows, we define the Nyquist frequency of the QAM system to be 800 MHz. The experimental data were sampled using the FRI-based method with the same spatial step size but with temporal sampling frequencies ranging from 75 MHz to 250 MHz (25 MHz steps) yielding from 7 to 21 samples per RF line. These sampling frequencies correspond to a range from approximately 9.4% to 31.3% of the QAM system Nyquist frequency 800 MHz.

F. *Similarity measures*

Quantitative evaluations between the acoustic maps obtained with the proposed approach and their counterpart produced from fully sampled RF signals are performed using the normalized mean squared error (**NRMSE**= $\sqrt{\frac{\|\mathbf{x}-\hat{\mathbf{x}}\|^2}{\|\mathbf{x}\|^2}}$) and the peak signal to noise ratio (**PSNR(dB)**= $10\log_{10}\frac{\max(\mathbf{x},\hat{\mathbf{x}})^2}{\|\mathbf{x}-\hat{\mathbf{x}}\|^2}$), which are defined as the comparison between two images $\mathbf{x}$ and $\hat{\mathbf{x}}$.

IV. Simulation Results

Simulations were conducted with nine innovation rates chosen considering 6 dB bandwidth of the reference signal, based on the methods introduced in Section III. The results are reported in Section IV-A for the Fourier coefficients estimation and subsequently in Section IV-B for the acoustic parameter estimation. More importantly, the outcomes in the second part lead to an instructive discussion on how the most preferable innovation rate could be selected in a sense of the sampling efficiency and the estimation accuracy.

A. *Estimation of Fourier coefficients*

The first step following QAM RF signal sampling at innovation rate is to recover the discrete Fourier coefficients $X[k]$ as described in (11)-(14). Fig. 4 depicts the comparison between the Fourier coefficients estimated by the proposed method and those computed by the conventional sampling scheme separately in the real and imaginary parts. The illustrative results demonstrate that there is no visually perceptible discrepancy caused by the FRI estimation method. Table I shows the average and the standard deviation (over $10,000$ recovered

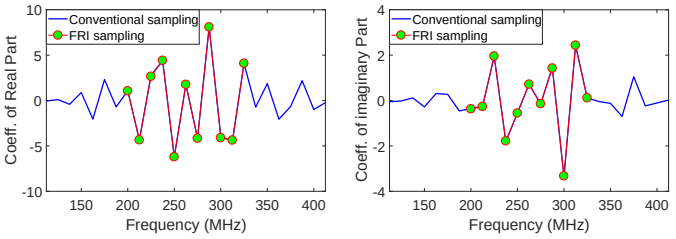

(a) (b)

Fig. 4. Real parts (a) and imaginary parts (b) of FT coefficients estimated from FRI sampling scheme (11 samples, *i.e.* 125 MHz) are overlapped on the FT coefficients acquired by conventional sampling (200 samples, *i.e.* 2.5 GHz).

signals) of the normalized root mean squared error relative to the Fourier coefficients obtained using the FRI approach. Overall, the numerical comparison confirms that the Fourier coefficients are estimated nearly perfectly, which is consistent with the qualitative observations of Fig. 4. Evidently, it can be expected that the accurate recovery of the Fourier coefficients will contribute to the exact estimation of acoustic parameters as revealed in the following section. In addition, it turns out that the estimation error depends on the design of the SoS sampling kernel, in particular being affected by the selection of the window function, *i.e.* b_k's in (10), and the strategy for finding the optimal window coefficients is referred to in [17].

B. Acoustic parameter maps

We herein evaluate the quality of the 2D acoustic maps, *i.e.* speed of sound map (2DcM) and acoustic impedance map (2DZM), reconstructed from QAM RF signals sampled following the proposed scheme against the one estimated from fully sampled RF data cubes. Fig. 5 (a) and (b-i) shows 2DcMs reconstructed from the conventional AR estimator (*i.e.*, applied to the data sampled at 2.5 GHz) and using the proposed FRI-based AR estimator applied at 8 different effective innovation rates. Similarly, Fig. 6 shows the red boxes of Fig. 5 to provide visual details at a finer scale. On the whole, in spite of the innovation rate sampling, the 2DcMs reconstructed using the FRI-based AR estimator shows no significant visual degradation except for the 2DcM built from 7 samples (*i.e.*, sampling at 75.0 MHz) of Fig. 5 (b). Additionally, Fig. 7 compares the single lines extracted at 0.4mm on the y-axis of each map in order to scrutinize the estimation accuracy of the acoustic parameter in the 2DcMs yielded from the innovation rates. It clearly illustrates two lines are exactly overlapped on most positions in the sampling schemes using over 125.0 MHz of Fig. 7 (c)-(h), whereas the result recovered from 75.0 MHz reveals the severe distortion as observed earlier. Figures 8, 9 and 10 present the 2DZM results in the exact same fashion as Figures 5, 6, and 7. Overall, the results follow the same trends as those of the 2DcMs. The above visual observations are quantitatively confirmed by standard quality metrics (*i.e.*, normalized root mean square error and peak signal to noise ratio) shown in the Table II (which were computed in the zoomed in areas, *i.e.*, red rectangle). As expected, the results obtained with 7 samples show large NRMSE and low PSNR. Small improvement exists in these metrics when 9 samples are used. Interestingly, NRMSE and PSNR results for between 11 and 21 samples are all satisfactory and nearly identical. No further improvement is obtained even when more samples are used, which will be discussed in the following section.

V. Discussion and Conclusions

The objective of this work was to combine the innovation rate sampling procedure of RF signal with the AR model-based parametric acoustic map reconstruction in QAM imaging. Both approaches were based on a parametric model of the QAM RF signals with a limited number of degrees of freedom, *i.e.* the amplitudes, time delays and frequency-dependent attenuation coefficients. We showed encouraging results by proving that the proposed FRI-based AR approach can reconstruct 2D acoustic maps with an accuracy comparable to the conventional QAM technology, despite using sampling frequency 18 times lower than the one (2.5 GHz) classically used within existing imaging systems and 6 times lower than the rate (800 MHz) required by the Nyquist criterion.

Taking into account a model mismatch caused by noise, artifacts or scattering in the tissue structure, the FRI-based AR estimator is able to obtain the most desirable two echoes in the manner of screening out such noise perturbations with the dedicated logic. In this sense, increasing n in (16) implies that we can construct more individual pulses, and two correct reflections are more likely to be separable from the noise effects. However, because this requires the increase of Fourier coefficients, *i.e.* higher innovation rate, we need to find a compromise. Except for the results acquired from the innovation rates below 6-dB bandwidth, *i.e.* 7 and 9 samples, the overall numerical assessments on the Table II reveal no noticeable improvement even though the number of samples increases. This is likely to result from the fact that, as illustrated in the Fig. 2(b), the coefficients away from the center frequency have less contribution to the signal information. Accordingly, the analysis of the power distribution of a reference signal could offer a critical insight to determine the most relevant innovation rate of a QAM RF signal featured by five parameters. Likewise, the estimation failure in less innovation rates than 11 samples could be explained in this perspective. To conclude, the simulation results legitimize that the innovation rate (125 MHz) of 11 samples, equivalent to 6 dB bandwidth showing the estimation performance comparable to its counterparts (*i.e.* over 125 MHz), can be considered as the optimal operating in this experiment, *i.e.* the compromise between the sampling cost and the image quality as stated above.

Strang-Fix condition [25], [26] defines the property of a sampling kernel able to perfectly represent the moments of an FRI signal in a subspace spanned with a maximum order corresponding to the innovation rate. In the simulations, we used SoS sampling kernel in [17] since it respects this property. However, other sampling kernels could also be considered such as B-splines that reproduce polynomials other than exponentials [29], [30].

The FRI-based AR approach to QAM presented in this paper has tremendous implications for QAM systems. For instance,

Number of samples		7	9	11	13	15	17	19	21
Sampling frequency (MHz)		75	100	125	150	175	200	225	250
Fraction of Nyquist rate (800 MHz) in %		9.4	12.5	15.6	18.8	21.9	25.0	28.1	31.3
Real part of FT coefficients	NRMSE	0.0137	0.0126	0.0132	0.0116	0.0100	0.0090	0.0089	0.0089
	STD.	0.0063	0.0055	0.0048	0.0057	0.0045	0.0037	0.0034	0.0032
Imaginary part of FT coefficients	NRMSE	0.0064	0.0062	0.0067	0.0060	0.0058	0.0056	0.0059	0.0058
	STD.	0.0020	0.0021	0.0022	0.0028	0.0023	0.0023	0.0022	0.0022

TABLE I
The average and standard deviation of normalized root mean squared error (over 10,000 recovered signals) with respect to real and imaginary parts of FT coefficients retrieved from various innovation rates

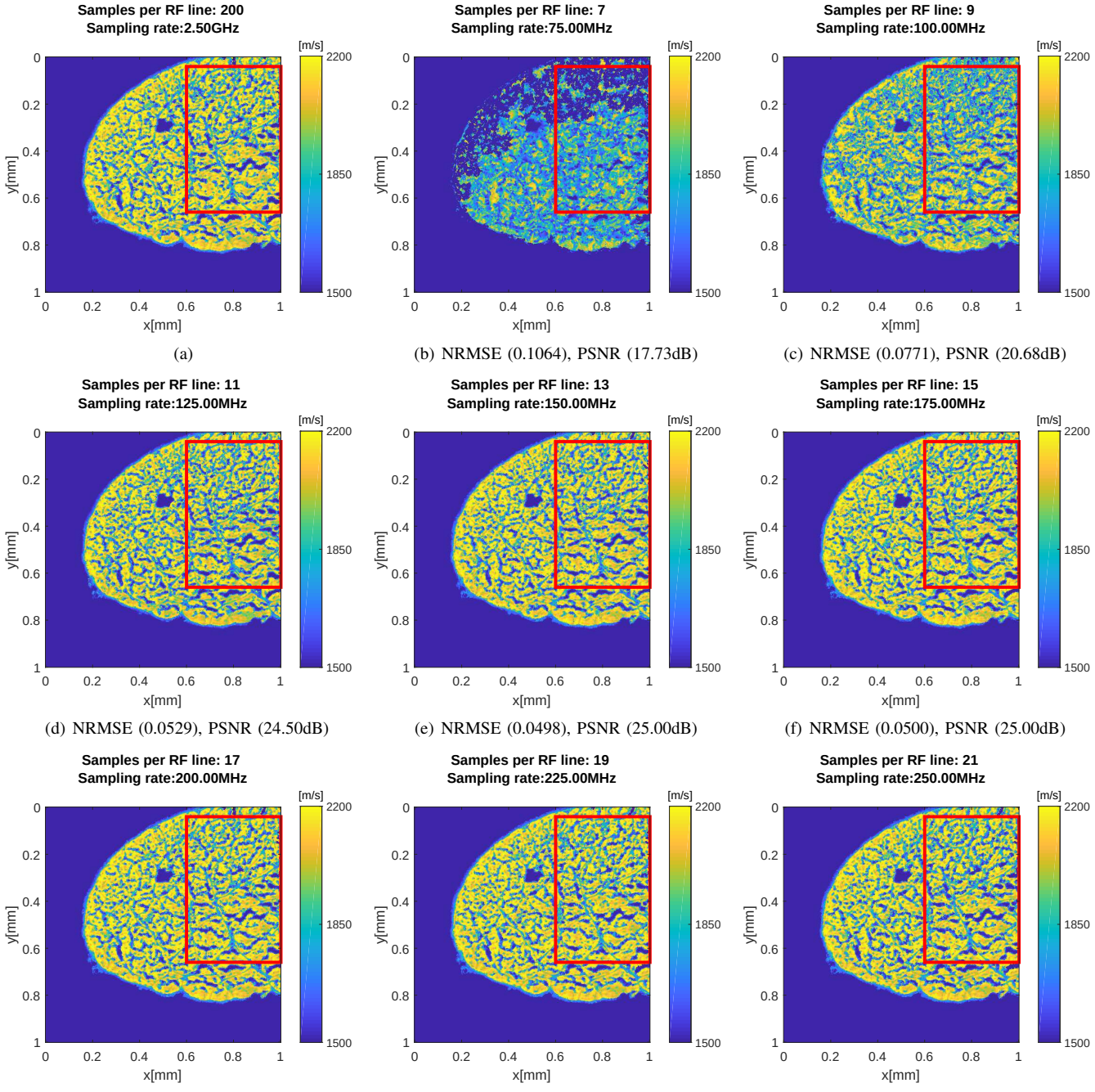

(a)

(b) NRMSE (0.1064), PSNR (17.73dB)

(c) NRMSE (0.0771), PSNR (20.68dB)

(d) NRMSE (0.0529), PSNR (24.50dB)

(e) NRMSE (0.0498), PSNR (25.00dB)

(f) NRMSE (0.0500), PSNR (25.00dB)

(g) NRMSE (0.0498), PSNR (25.07dB)

(h) NRMSE (0.0493), PSNR (25.16dB)

(i) NRMSE (0.0509), PSNR (24.87dB)

Fig. 5. (a) and (b-i) are speed of sound maps estimated from fully-sampled RF data cube (200 samples per RF signal), and from samples acquired following the proposed approach corresponding to respectively 7, 9, 11, 13, 15, 17, 19 and 21 samples per RF signal. Quantitative accuracy measurements computed from the red box in these speed of sound maps are given in Table II.

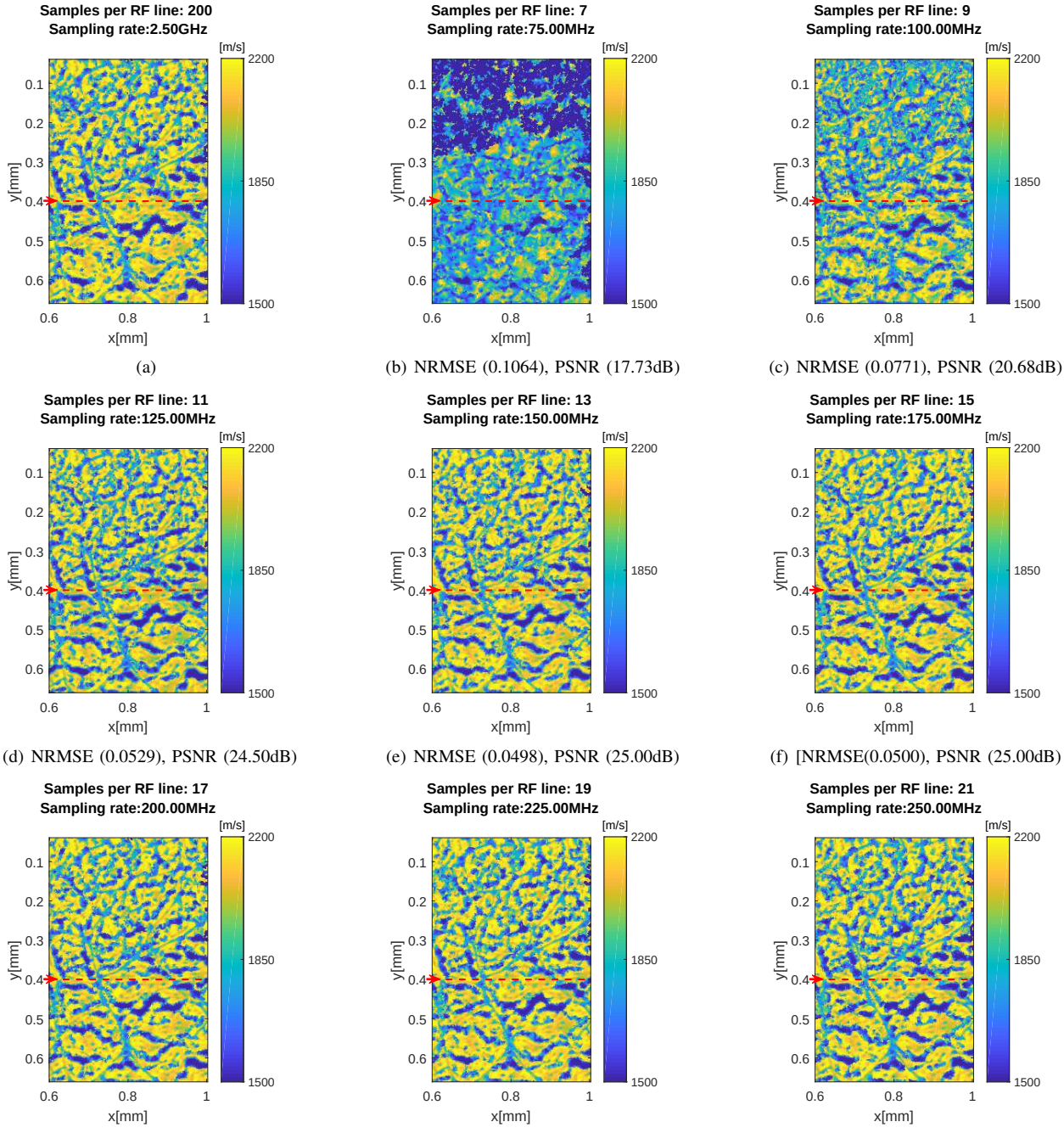

(a)

(b) NRMSE (0.1064), PSNR (17.73dB)

(c) NRMSE (0.0771), PSNR (20.68dB)

(d) NRMSE (0.0529), PSNR (24.50dB)

(e) NRMSE (0.0498), PSNR (25.00dB)

(f) [NRMSE(0.0500), PSNR (25.00dB)

(g) NRMSE (0.0498), PSNR (25.07dB)

(h) NRMSE (0.0493), PSNR (25.16dB)

(i) NRMSE (0.0509), PSNR (24.87dB)

Fig. 6. Magnified maps of the red boxes in Fig. 5. (a) is the SOS map created from fully-sampled RF data cube (200 samples per RF signal), (b-i) are the SOS maps estimated following the proposed approach corresponding to respectively 7, 9, 11, 13, 15, 17, 19 and 21 samples per RF signal. The red dotted line indicates the cross sectioned location of profiles in Fig. 7.

Number of samples		7	9	11	13	15	17	19	21
Sampling frequency (MHz)		75	100	125	150	175	200	225	250
Fraction of Nyquist rate (800 MHz) in %		9.4	12.5	15.6	18.8	21.9	25.0	28.1	31.3
Speed of sound map	NRMSE	0.1064	0.0771	0.0529	0.0498	0.0500	0.0498	0.0493	0.0509
	PSNR(dB)	17.73	20.68	24.50	25.00	25.00	25.07	25.16	24.87
Acoustic impedance map	NRMSE	0.1073	0.0842	0.0591	0.0631	0.0498	0.0464	0.0461	0.0456
	PSNR(dB)	18.41	21.42	24.51	23.94	25.99	26.60	26.66	26.74

TABLE II

Quantitative results computed between the 2D map from fully sampled RF data cube and those obtained from QAM RF signal sampled at low rates: 262.5 MHz (21 samples per RF signal), 237.5 MHz (19 samples per RF signal), 212.5 MHz (17 samples per RF signal), 187.5 MHz (15 samples per RF signal),162.5 MHz (13 samples per RF signal), 137.5 MHz (11 samples per RF signal), 112.5 MHz (9 samples per RF signal) and 87.5 MHz (7 samples per RF signal) .

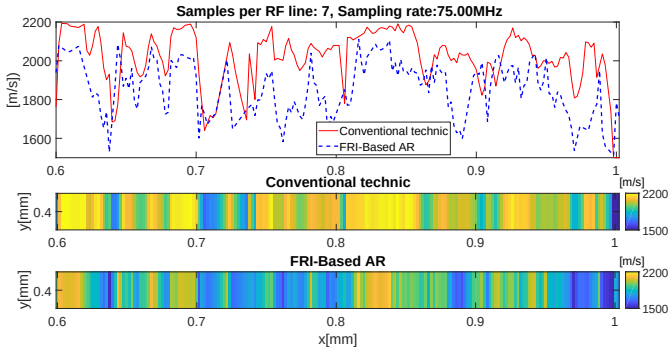

(a) NRMSE (0.1140), PSNR (18.89)

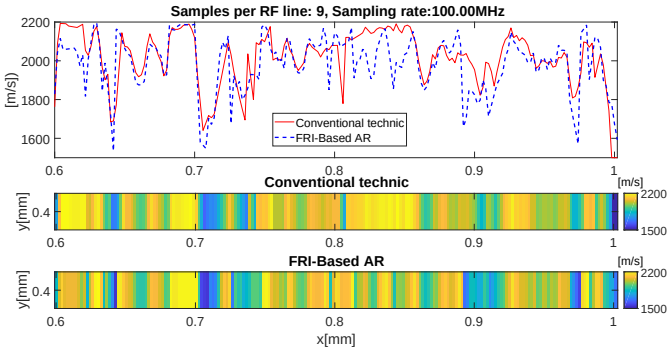

(b) NRMSE (0.0520), PSNR (25.61)

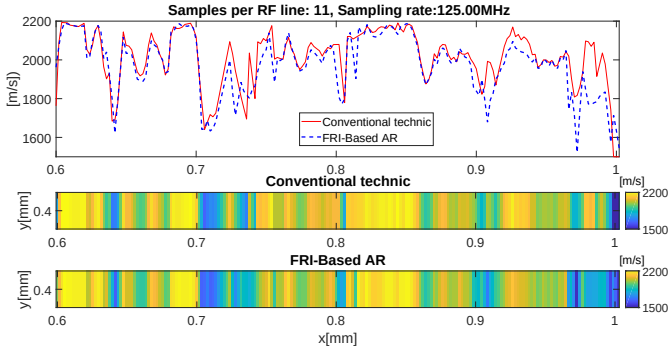

(c) NRMSE (0.0300), PSNR (30.33)

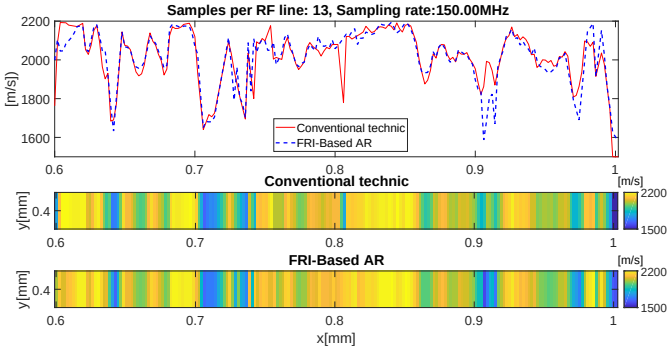

(d) NRMSE (0.0274), PSNR (31.24)

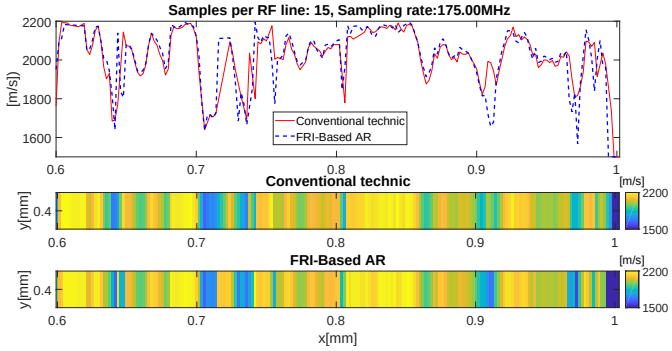

(e) NRMSE (0.0354), PSNR (29.10)

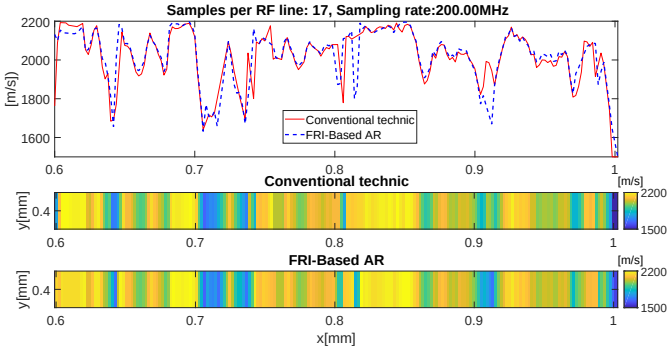

(f) NRMSE (0.0284), PSNR (31.02)

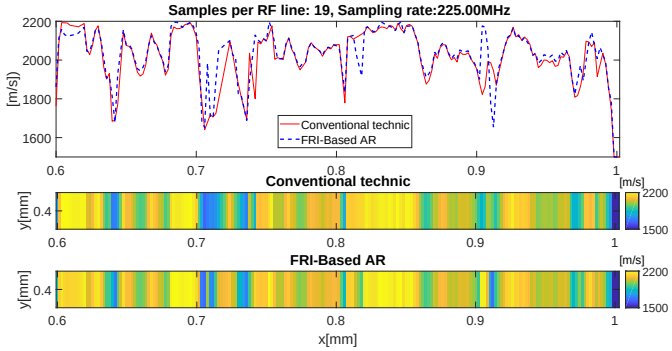

(g) NRMSE (0.0243), PSNR (32.45)

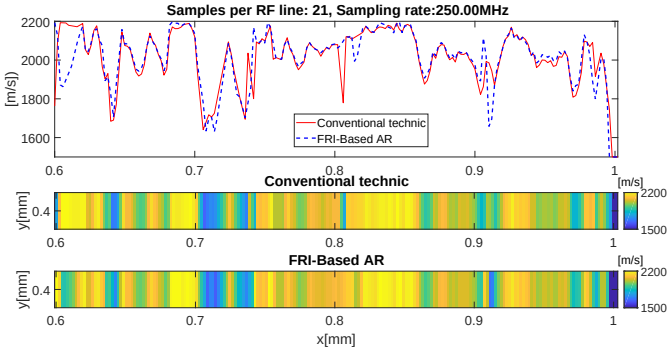

(h) NRMSE (0.0267), PSNR (31.54)

Fig. 7. Horizontal cross sections and single lines of 2DcM at 0.4mm of y-axis in Fig. 6. The red continuous lines are a cross section from fully sampled map, *i.e.* Fig. 6(a) which is used as the criterion for comparison. The blue dotted lines of (a-h) represent the cross sections of Fig. 6(b-i) respectively.

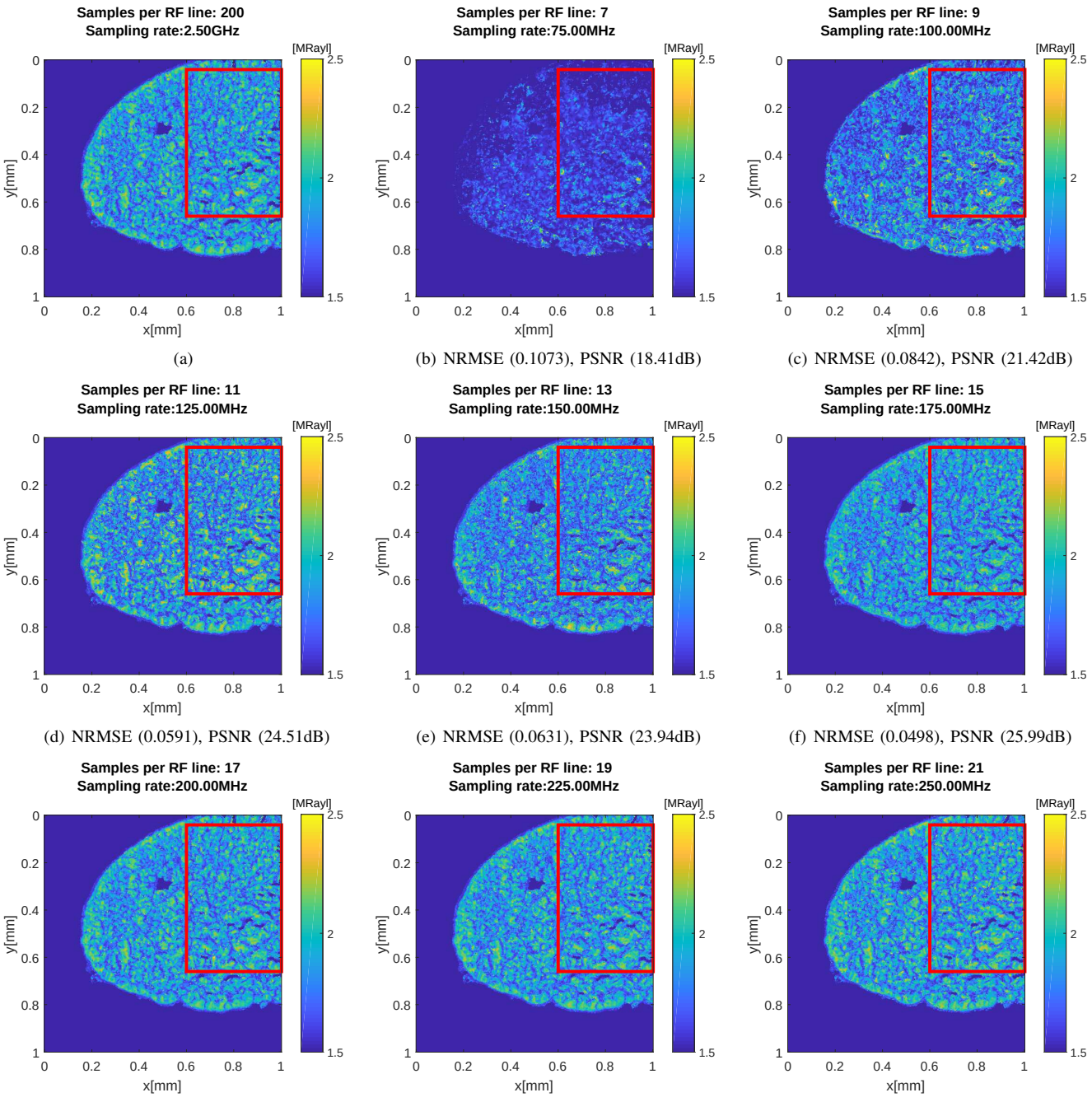

(a)

(b) NRMSE (0.1073), PSNR (18.41dB)

(c) NRMSE (0.0842), PSNR (21.42dB)

(d) NRMSE (0.0591), PSNR (24.51dB)

(e) NRMSE (0.0631), PSNR (23.94dB)

(f) NRMSE (0.0498), PSNR (25.99dB)

(g) NRMSE (0.0464), PSNR (26.60dB)

(h) NRMSE (0.0461), PSNR (26.66dB)

(i) NRMSE (0.0456), PSNR (26.74dB)

Fig. 8. (a) and (b-i) are acoustic impedance maps estimated from fully-sampled RF data cube (200 samples per RF signal), and from RF signals sampled following the proposed approach corresponding to respectively 7, 9, 11, 13, 15, 17, 19 and 21 samples per RF signal. Quantitative accuracy measurements computed from the red box in these speed of sound maps are given in Table II.

it would allow the use of much slower A/D cards than those currently used. This would drastically reduce costs. Furthermore, slower A/D cards are much easier to manufacture and therefore can be made with higher bit counts (*e.g.*, 16 bits sampling at 250 MHz is much easier to manufacture than 12 bits at 2.5 GHz) yielding increased data quality and lower sensitivity to noise. Currently, most QAM systems do not fully operate in real-time and require a few seconds to process the data and form images. The FRI-based AR approach completely short circuits the process of forming images by not only providing much less data overall, but, more importantly, by directly providing normalized Fourier coefficients used in the AR algorithm thus saving precious computation time.

Based on this achievement, we plan to propose an approach able to further reduce the data acquisition time and the size of the data cube from spatio-temporally under-sampled measurements by combining both the compressed sensing framework [31], [32] and the finite rate of innovation signal theory. The integration of two methods is straightforward thanks to the previous study [6]; the compressed scanning scheme in spatial

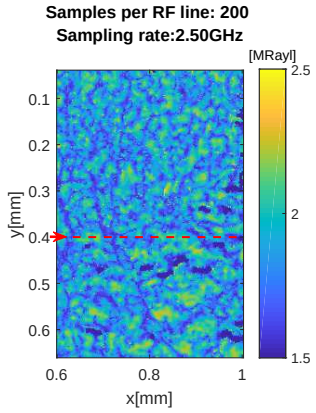

(a)

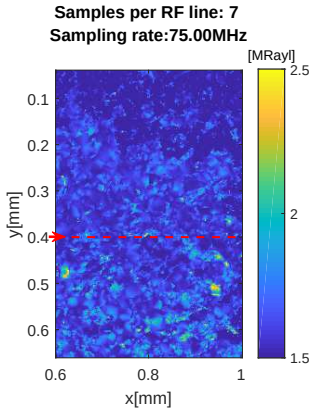

(b) NRMSE (0.1073), PSNR (18.41dB)

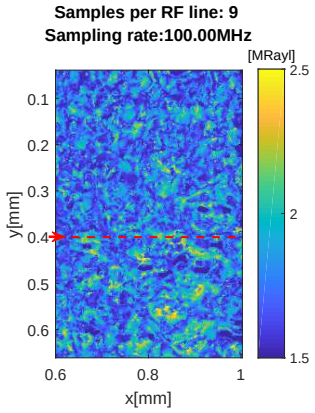

(c) NRMSE (0.0842), PSNR (21.42dB)

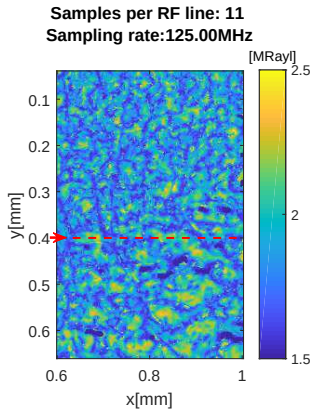

(d) NRMSE (0.0591), PSNR (24.51dB)

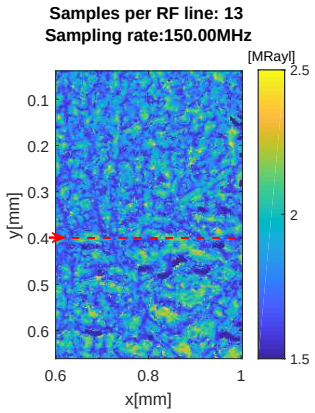

(e) NRMSE (0.0631), PSNR (23.94dB)

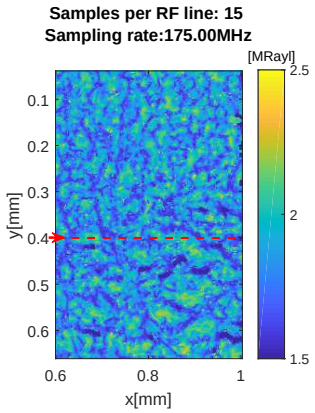

(f) NRMSE (0.0498), PSNR (25.99dB)

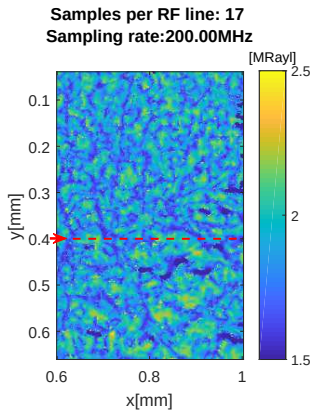

(g) NRMSE (0.0464), PSNR (26.60dB)

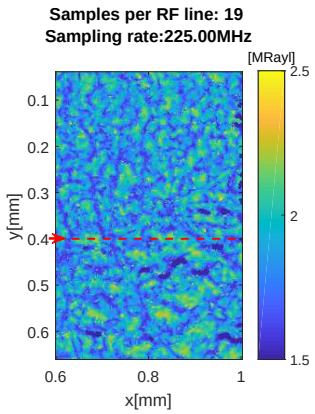

(h) NRMSE (0.0461), PSNR (26.66dB)

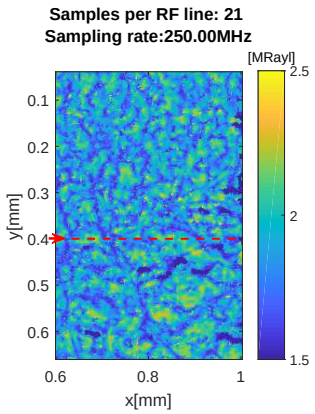

(i) NRMSE (0.0456), PSNR (26.74dB)

Fig. 9. Magnified maps of the red boxes in Fig. 5. (a) is the acoustic impedance map created from fully-sampled RF data cube (200 samples per RF signal), (b-i) are the SOS maps estimated following the proposed approach corresponding to respectively 7, 9, 11, 13, 15, 17, 19 and 21 samples per RF signal. The red dotted line indicates the cross sectioned location of profiles in Fig. 10.

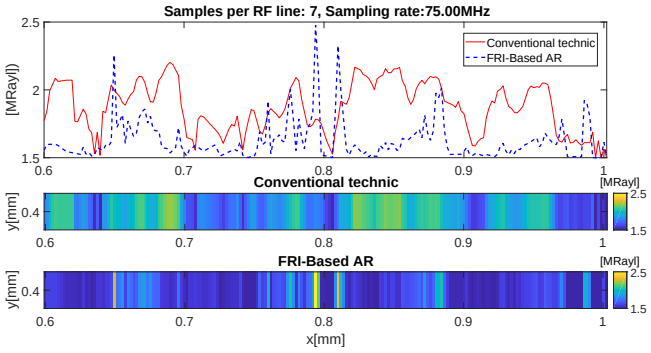

(a) NRMSE (0.1460), PSNR (16.69dB)

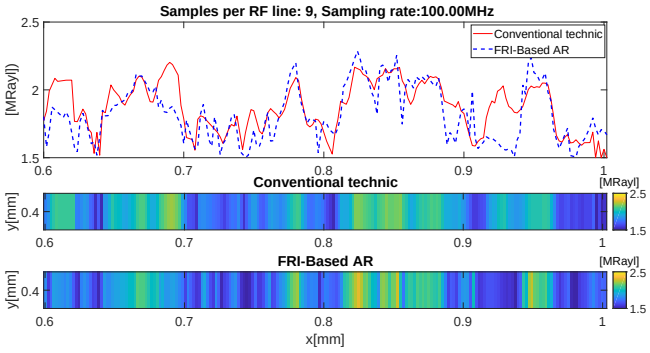

(b) NRMSE (0.1000), PSNR (19.97dB)

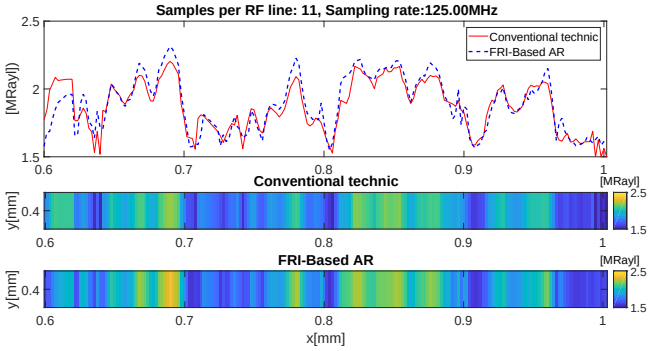

(c) NRMSE (0.0540), PSNR (25.31dB)

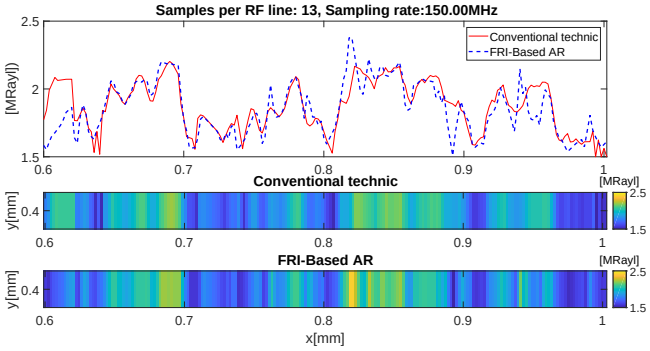

(d) NRMSE (0.0590), PSNR (24.54dB)

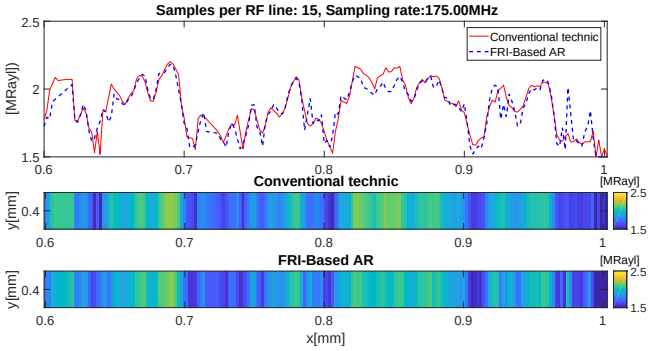

(e) NRMSE (0.0430), PSNR (27.31dB)

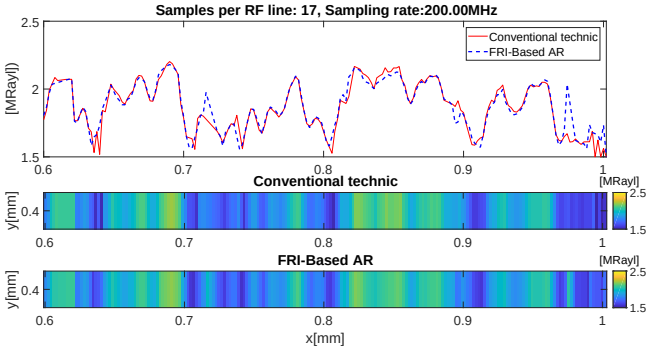

(f) NRMSE (0.0390), PSNR (28.12dB)

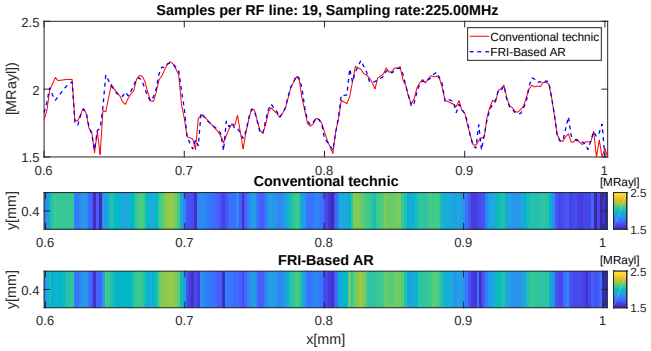

(g) NRMSE (0.0400), PSNR (27.96dB)

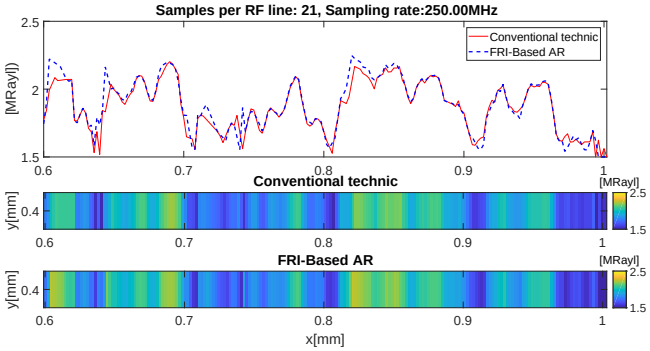

(h) NRMSE (0.0350), PSNR (29.20dB)

Fig. 10. Horizontal cross sections and single lines of 2DZM at 0.4mm of y-axis in Fig. 9. The red continuous lines are a cross section from fully sampled map, *i.e.* Fig. 9(a) which is used as the criterion for comparison. The blue dotted lines of (a-h) represent the cross sections of Fig. 9(b-i) respectively.

domain followed by the FRI sampling in temporal domain will lead to extremely squashed data cube compared to the conventional QAM technique.

VI. Acknowledgments

The authors wish to thank Prof. Ian A Sigal, Dr. Bin Yang, and Mr. Po Lam from the Ocular Biomechanics Laboratory at the University of Pittsburgh for preparing and providing the chicken tendon samples. The authors also thank Mr. Takuya Ogawa from Chiba University in Chiba, Japan for experimental help.

References

[1] S. Irie, K. Inoue, K. Yoshida, J. Mamou, K. Kobayashi, H. Maruyama, and T. Yamaguchi, "Speed of sound in diseased liver observed by scanning acoustic microscopy with 80 mhz and 250 mhz," *The Journal of the Acoustical Society of America*, vol. 139, no. 1, pp. 512–519, 2016.

[2] J. Mamou, D. Rohrbach, E. Saegusa-Beecroft, E. Yanagihara, J. Machi, and E. J. Feleppa, "Ultrasound-scattering models based on quantitative acoustic microscopy of fresh samples and unstained fixed sections from cancerous human lymph nodes," in *2015 IEEE International Ultrasonics Symposium (IUS)*, pp. 1–4, Oct 2015.

[3] D. Rohrbach, H. O. Lloyd, R. H. Silverman, R. Urs, and J. Mamou, "Acoustic-property maps of the cornea for improved high-frequency ultrasound corneal biometric accuracy," in *2015 IEEE International Ultrasonics Symposium (IUS)*, pp. 1–4, Oct 2015.

[4] D. Rohrbach, A. Jakob, H. O. Lloyd, S. H. Tretbar, R. H. Silverman, and J. Mamou, "A novel quantitative 500-mhz acoustic microscopy system for ophthalmologic tissues," *IEEE Transactions on Biomedical Engineering*, vol. 64, pp. 715–724, March 2017.

[5] D. Rohrbach and J. Mamou, "Autoregressive signal processing applied to high-frequency acoustic microscopy of soft tissues," *IEEE Transactions on Ultrasonics, Ferroelectrics, and Frequency Control*, vol. 65, pp. 2054–2072, Nov 2018.

[6] J. Kim, J. Mamou, P. R. Hill, N. Canagarajah, D. Kouamé, A. Basarab, and A. Achim, "Approximate message passing reconstruction of quantitative acoustic microscopy images," *IEEE Transactions on Ultrasonics, Ferroelectrics, and Frequency Control*, vol. 65, pp. 327–338, March 2018.

[7] J.-H. Kim, J. Mamou, D. Kouamé, A. Achim, and A. Basarab, "Reconstruction of Quantitative Acoustic Microscopy Images from RF Signals Sampled at Innovation Rate," in *IEEE International Ultrasonics Symposium, Kobe, Japan*, pp. 1–4, octobre 2018.

[8] M. Vetterli, P. Marziliano, and T. Blu, "Sampling signals with finite rate of innovation," *IEEE Transactions on Signal Processing*, vol. 50, pp. 1417–1428, Jun 2002.

[9] Y. M. Lu and M. N. Do, "A theory for sampling signals from a union of subspaces," *IEEE Transactions on Signal Processing*, vol. 56, pp. 2334–2345, June 2008.

[10] P. Stoica and R. Moses, *Introduction to Spectral Analysis*. Engle-wood Cliffs, NJ: Prentice-Hall, 2000.

[11] Y. Hua and T. K. Sarkar, "Matrix pencil method for estimating parameters of exponentially damped/undamped sinusoids in noise," *IEEE Transactions on Acoustics, Speech, and Signal Processing*, vol. 38, pp. 814–824, May 1990.

[12] M. Elad, P. Milanfar, and G. H. Golub, "Shape from moments - an estimation theory perspective," *IEEE Transactions on Signal Processing*, vol. 52, pp. 1814–1829, July 2004.

[13] J. Oñativia, S. R. Schultz, and P. L. Dragotti, "A finite rate of innovation algorithm for fast and accurate spike detection from two-photon calcium imaging," *Journal of Neural Engineering*, vol. 10, no. 4, p. 046017, 2013.

[14] S. Rudresh and C. S. Seelamantula, "Finite-rate-of-innovation-sampling-based super-resolution radar imaging," *IEEE Transactions on Signal Processing*, vol. 65, pp. 5021–5033, Oct 2017.

[15] X. Wei and P. L. Dragotti, "Fresh x2014;fri-based single-image super-resolution algorithm," *IEEE Transactions on Image Processing*, vol. 25, pp. 3723–3735, Aug 2016.

[16] H. Pan, T. Blu, and M. Vetterli, "Towards generalized fri sampling with an application to source resolution in radioastronomy," *IEEE Transactions on Signal Processing*, vol. 65, pp. 821–835, Feb 2017.

[17] R. Tur, Y. C. Eldar, and Z. Friedman, "Innovation rate sampling of pulse streams with application to ultrasound imaging," *IEEE Transactions on Signal Processing*, vol. 59, pp. 1827–1842, April 2011.

[18] I. Maravic and M. Vetterli, "Sampling and reconstruction of signals with finite rate of innovation in the presence of noise," *IEEE Transactions on Signal Processing*, vol. 53, pp. 2788–2805, Aug 2005.

[19] P. L. Dragotti, M. Vetterli, and T. Blu, "Exact sampling results for signals with finite rate of innovation using strang-fix conditions and local kernels," in *Proceedings. (ICASSP '05). IEEE International Conference on Acoustics, Speech, and Signal Processing, 2005.*, vol. 4, pp. iv/233–iv/236 Vol. 4, March 2005.

[20] J. Urigüen, "Exact and approximate strang-fix conditions to reconstruct signals with finite rate of innovation from samples taken with arbitrary kernels," Sep 2013.

[21] G. Strang and G. Fix, "A fourier analysis of the finite element variational method," in *Constructive Aspect of Functional Analysis*, pp. 796–830, Rome, Italy: Edizioni Cremonese, 1971.

[22] M. Unser and T. Blu, "Cardinal exponential splines: part i - theory and filtering algorithms," *IEEE Transactions on Signal Processing*, vol. 53, pp. 1425–1438, April 2005.

[23] B. Porat, *A course in Digital Signal Processing*. New York: Wiley, 1997.

[24] J. Kirkhorn, "Introduction to IQ-demodulation of RF-data," *Tech. Rep., IFBT, NTNU*, Sep 1999.

[25] M. U. Ildar Khalidov, Thierry Blu, "Generalized l-spline wavelet bases," 2005.

[26] C. Vonesch, T. Blu, and M. Unser, "Generalized daubechies wavelet families," *IEEE Transactions on Signal Processing*, vol. 55, pp. 4415–4429, Sep. 2007.

[27] B. Yang, N.-J. Jan, B. Brazile, A. Voorhees, K. L. Lathrop, and I. A. Sigal, "Polarized light microscopy for 3-dimensional mapping of collagen fiber architecture in ocular tissues," *Journal of biophotonics*, vol. 11, no. 8, p. e201700356, 2018.

[28] D. Rohrbach, H. O. Lloyd, R. H. Silverman, and J. Mamou, "Fine-resolution maps of acoustic properties at 250 mhz of unstained fixed murine retinal layers," *The Journal of the Acoustical Society of America*, vol. 137, no. 5, pp. EL381–EL387, 2015.

[29] M. Unser, "Splines: a perfect fit for signal and image processing," *IEEE Signal Processing Magazine*, vol. 16, pp. 22–38, Nov 1999.

[30] P. L. Dragotti, M. Vetterli, and T. Blu, "Sampling moments and reconstructing signals of finite rate of innovation: Shannon meets strang-fix," *IEEE Transactions on Signal Processing*, vol. 55, pp. 1741–1757, May 2007.

[31] E. J. Candes, J. Romberg, and T. Tao, "Robust uncertainty principles: exact signal reconstruction from highly incomplete frequency information," *IEEE Transactions on Information Theory*, vol. 52, pp. 489–509, Feb 2006.

[32] D. L. Donoho, "Compressed sensing," *IEEE Transactions on Information Theory*, vol. 52, pp. 1289–1306, April 2006.